THE
UNIVERSITY
OF RHODE ISLAND

University of Rhode Island
DigitalCommons@URI

Graduate School of Oceanography Faculty
Publications

Graduate School of Oceanography

1999

Ozone and aerosol distributions and air mass characteristics over the South Pacific during the burning season

Marta A. Fenn

Edward V. Browell

See next page for additional authors

Follow this and additional works at: https://digitalcommons.uri.edu/gsofacpubs

Authors

Marta A. Fenn, Edward V. Browell, Carolyn F. Butler, William B. Grant, Susan A. Kooi, Marian B. Clayton, Gerald L. Gregory, Reginald E. Newell, Yong Zhu, Jack E. Dibb, Henry E. Fuelberg, Bruce E. Anderson, Alan R. Bandy, Donald R. Blake, John D. Bradshaw, Brian G. Heikes, Glen W. Sachse, Scott T. Sandholm, Hanwant B. Singh, Robert W. Talbot, and Donald C. Thornton

Ozone and aerosol distributions and air mass characteristics over the South Pacific during the burning season

Marta A. Fenn,[1] Edward V. Browell,[2] Carolyn F. Butler,[1] William B. Grant,[2]
Susan A. Kooi,[1] Marian B. Clayton,[1] Gerald L. Gregory,[2] Reginald E. Newell,[3]
Yong Zhu,[3] Jack E. Dibb,[4] Henry E. Fuelberg,[5] Bruce E. Anderson,[2] Alan R. Bandy,[6]
Donald R. Blake,[7] John D. Bradshaw,[8] Brian G. Heikes,[9] Glen W. Sachse,[2]
Scott T. Sandholm,[8] Hanwant B. Singh,[10] Robert W. Talbot,[4] and Donald C. Thornton[6]

Abstract. In situ and laser remote measurements of gases and aerosols were made with airborne instrumentation to establish a baseline chemical signature of the atmosphere above the South Pacific Ocean during the NASA Global Tropospheric Experiment (GTE)/Pacific Exploratory Mission-Tropics A (PEM-Tropics A) conducted in August–October 1996. This paper discusses general characteristics of the air masses encountered during this experiment using an airborne lidar system for measurements of the large-scale variations in ozone (O_3) and aerosol distributions across the troposphere, calculated potential vorticity (PV) from the European Centre for Medium-Range Weather Forecasting (ECMWF), and in situ measurements for comprehensive air mass composition. Between 8°S and 52°S, biomass burning plumes containing elevated levels of O_3, over 100 ppbv, were frequently encountered by the aircraft at altitudes ranging from 2 to 9 km. Air with elevated O_3 was also observed remotely up to the tropopause, and these air masses were observed to have no enhanced aerosol loading. Frequently, these air masses had some enhanced PV associated with them, but not enough to explain the observed O_3 levels. A relationship between PV and O_3 was developed from cases of clearly defined O_3 from stratospheric origin, and this relationship was used to estimate the stratospheric contribution to the air masses containing elevated O_3 in the troposphere. The frequency of observation of the different air mass types and their average chemical composition is discussed in this paper.

1. Introduction

The Pacific Exploratory Mission–Tropics A (PEM-Tropics A) mission is the third in a series of Global Tropospheric Experiment (GTE) missions sponsored by NASA designed to study the troposphere above the Pacific Ocean. It was conducted from August 30 through October 5, 1996, during a period when the climatological flow in the southern hemisphere was from the west, providing the greatest distance from upwind continental sources. PEM-Tropics A was designed to provide a picture of the chemical state of this remote atmosphere. A primary objective of the

mission was to investigate the atmospheric chemistry of O_3 and its precursors in this photochemically and radiatively important region. To that end, two aircraft were deployed during PEM-Tropics A, NASA's DC-8 and P-3B, with instrumentation to measure over 75 trace and minor chemical species as well as meteorological parameters. NASA Langley Research Center's Airborne Ozone and Aerosol Lidar was carried by the DC-8 and was the only remote sensing instrument on either aircraft.

A total of 17 DC-8 flights were conducted as part of the PEM-Tropics A field experiment. A list of the flights, their objectives, and flight specific information is given in the overview paper by *Hoell et al.* [1999]. In situ measurements made at aircraft altitude (from the surface to 12.5 km) during PEM-Tropics A have revealed widespread occurrences of air having elevated O_3 and elevated O_3 precursors [*Talbot et al.*, 1999]. *Blake et al.* [this issue] report that the air masses with elevated O_3 precursors were not fresh and were derived from non-urban biomass combustion sources. *Fuelberg et al.* [1999] utilized kinematic back trajectory analyses [*Fuelberg et al.*, 1996] from several strong biomass burning plumes to identify possible source regions.

This study extends the air mass analysis possible at aircraft altitude over the entire troposphere. We report the results of a study of the large-scale characteristics of tropospheric air masses observed over the Southern Hemisphere Pacific during PEM-Tropics A using remotely determined O_3 and aerosols measurements together with potential vorticity (PV) fields derived from data provided by the European Centre for Medium-Range Weather Forecasting (ECMWF). We categorized observed air masses, determined the frequency of observation of those air

---
[1]Science Application International Corporation, Hampton, Virginia.

[2]NASA Langley Research Center, Hampton, Virginia.

[3]Department of Earth, Atmospheric and Planetary Sciences, Massachusetts Institute of Technology, Cambridge.

[4]Institute for the Study of Earth, Oceans, and Space, University of New Hampshire, Durham.

[5]Department of Meteorology, Florida State University, Tallahassee.

[6]Department of Chemistry, Drexell University, Philadelphia, Pennsylvania.

[7]Department of Chemistry, University of California, Irvine.

[8]School of Earth and Atmospheric Sciences, Georgia Institute of Technology, Atlanta.

[9]Graduate School of Oceanography, University of Rhode Island, Narragansett.

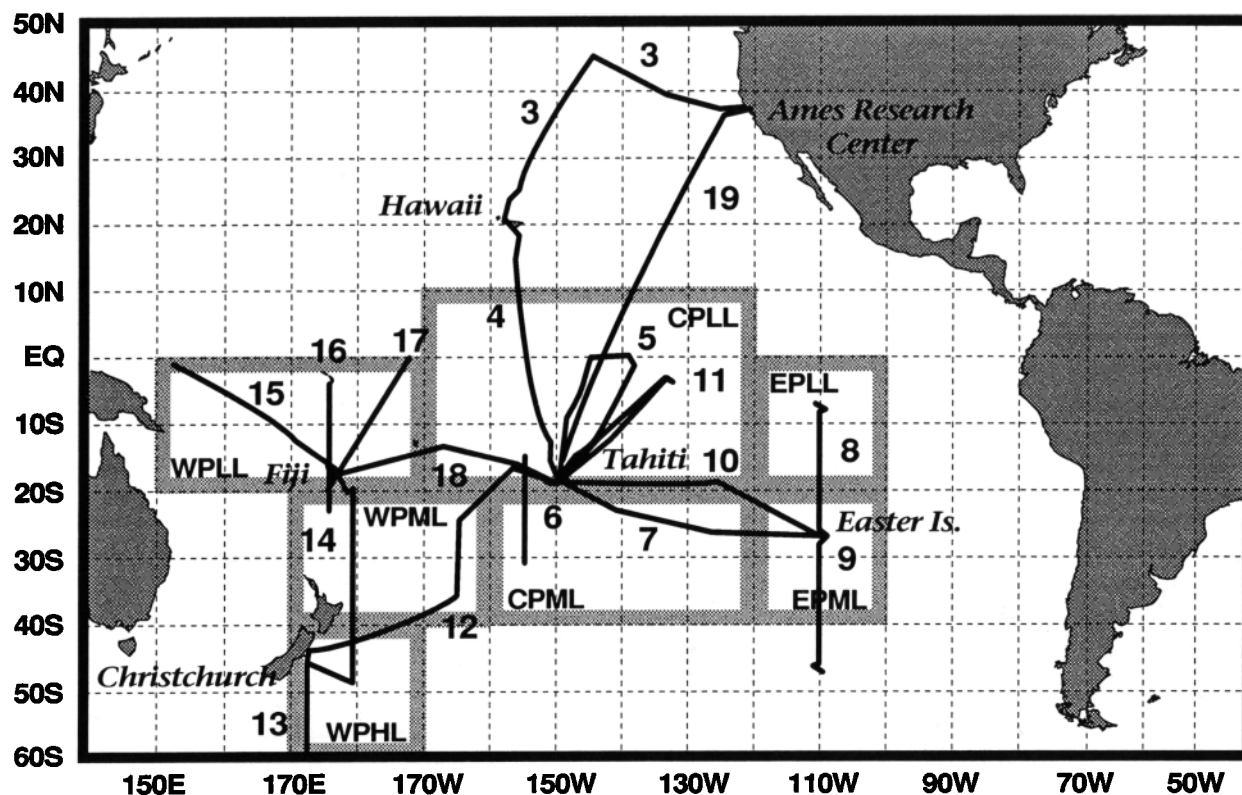[10]NASA Ames Research Center, Moffett Field, California.

Figure 1. Map of the PEM-Tropics A study region with flight tracks plotted. Flight numbers are marked. Shaded outlines mark regions used in air mass characterization: western Pacific low latitude (WPLL), western Pacific midlatitude (WPML), western Pacific high latitude (WPHL), central Pacific low latitude (CPLL), central Pacific midlatitude (CPML), eastern Pacific low latitude (EPLL), and eastern Pacific midlatitude (EPML).

masses over the Pacific, and calculated their average chemical composition.

2. Measurements and Model Data Products

2.1. Airborne Lidar Measurements

During this experiment, an airborne differential absorption lidar (DIAL) system collected both O_3 and aerosol data from near the surface to above the tropopause along the flight track of each flight, totaling over 120 hours of data collected between the latitudes 72°S and 45°N and longitudes 152°E and 110°W. The ground tracks for the flights are shown in Figure 1. Simultaneous zenith and nadir lidar measurements of O_3 and aerosols were made with a range of about 750 m above the aircraft to up to 6 km above the tropopause in the zenith case and from about 750 m below the aircraft to about 300 m above the surface in the nadir case. The DIAL O_3 measurements were made using an on-line wavelength of 288.20 nm and an off-line wavelength of 299.57 nm. Aerosol backscatter measurements were made at laser wavelengths of 1064 nm, ~600 nm, and ~300 nm.

An O_3 measurement accuracy of better than 10% or 2 ppbv, whichever is larger, with a vertical resolution of 300 m and a horizontal resolution of about 70 km (given 5-min averaging time and assuming an aircraft speed of about 233 m/s) was obtained with a precision of better than 5% or 1 ppbv [*Browell*, 1983; *Browell et al.*, 1983, 1985a, b]. The O_3 mixing ratio calculation utilizes molecular density information provided by ECMWF.

Comparisons between airborne DIAL and in situ O_3 measurements were made throughout PEM-Tropics A with a mean difference of 0.0 ppbv and standard deviation of difference of 6.0 ppbv for all aircraft spirals. An example of the comparison made around a upward spiral point during flight 6 is shown in Figure 2. The corresponding lidar cross section is shown in Plate 1 and is described in more detail at the end of this section.

The atmospheric scattering ratio (aerosol plus molecular scattering divided by molecular scattering) measurements were derived from the range-corrected lidar signal at the ~600-nm lidar wavelength using a modeled molecular scattering profile based on molecular density information from ECMWF normalized to an aerosol-free region along the lidar profile [see, e.g., *Collis and Russell*, 1976]. The atmospheric scattering ratio profile is not corrected for attenuation by the aerosols. The resolution of the atmospheric scattering ratio measurements is defined by the vertical averaging interval of 60 m, and the horizontal averaging interval of 2 s or ~470 m. The accuracy and precision of the atmospheric scattering ratio (1 plus aerosol scattering ratio) measurements with low aerosol extinction at ~600 nm are estimated to be better than 10%. Detailed characteristics of the current airborne DIAL system and the O_3 DIAL technique are given by *Browell* [1989], *Richter et al.* [1997], and *Browell et al.* [1998]. This system has been used in recent tropospheric field experiments over the remote Pacific during PEM-West A [*Browell et al.*, 1996a; *Fenn et al.*, 1997] and PEM-West B [*Fenn et al.*, 1997; *Newell et al.*, 1997] and over the tropical South Atlantic
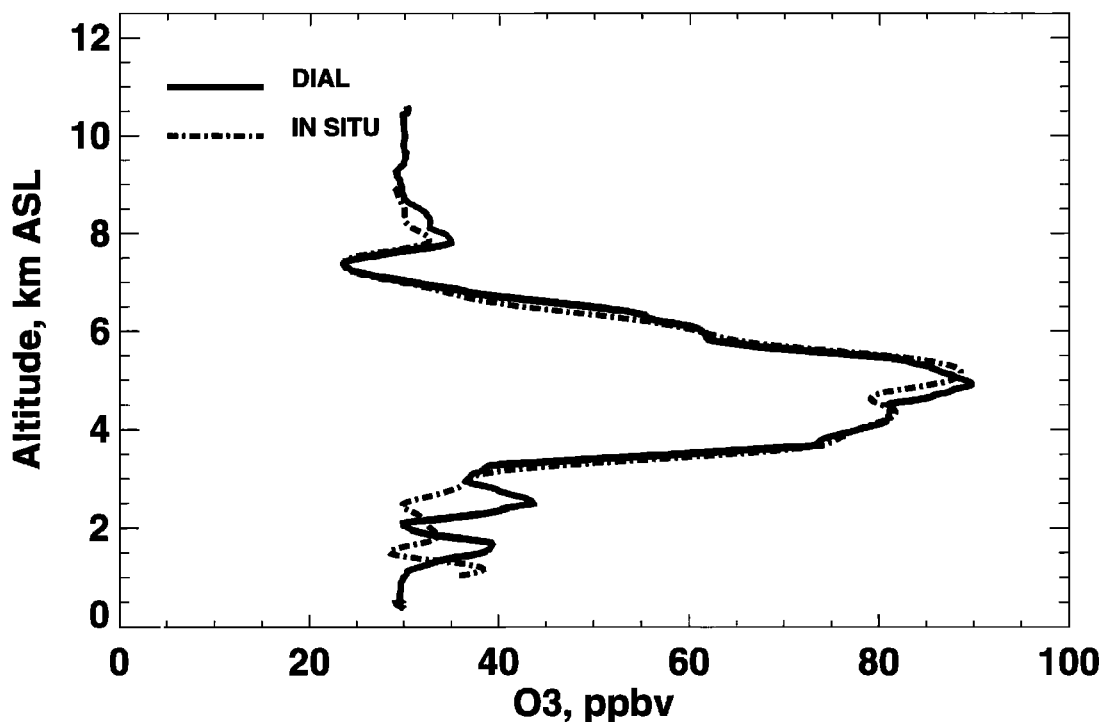
Figure 2. Vertical profiles of O_3 measured on September 5, 1996, at latitude 15.5°S and longitude 155°W by the DIAL instrument (solid line) and the in situ instrument (dashed line) within 50 min of each other. The time difference is less at the top. The average difference between the measurements is 1.3 ppbv, and the standard deviation of the difference is 4.1 ppbv.

Basin during Transport and Atmospheric Chemistry Near the Equatorial Atlantic (TRACE A) [*Browell et al.*, 1996b].

Plate 1 is an example of nadir O_3 and aerosol measurements made during flight 6. The marine boundary layer is less than 2 km in depth and is accompanied by O_3 values lower relative to the air above it. Optically thick clouds from 2220 to 2240 UT prevent the measurement of aerosols or O_3 below them. The region of elevated O_3 having mixing ratios in excess of 60 ppbv (3–6 km at the spiral point) constitutes a biomass burning plume unaccompanied by enhanced aerosol scattering. *Fuelberg et al.* [1999] describe the meteorology of this flight in detail and report that back trajectories from the center of this plume extend to southern Africa in 9–10 days, passing over the east coast of Australia 5 days before arriving at the flight track. They also report the in situ chemical signature of this biomass burning plume, and calculate it is approximately 5–7 days removed from the emission source.

Digital lidar data from all flights are available in the GTE web site at http://www-gte.larc.nasa.gov/, and images in Graphics Interchange Format (GIF) can be found on the Lidar Applications Group Home Page at http://asd-www.larc.nasa.gov/lidar/lidar. html. Results of the intercomparisons between DIAL O_3 and in situ O_3 are also available at both locations.

2.2. Tropospheric Ozone Cross Sections

Remote measurements of O_3 and aerosols provided nearly complete coverage of the entire troposphere along the aircraft track. In the case of the O_3 data, the 1500-m gap in the lidar measurements around the aircraft was filled in by an interpolation technique with the help of in situ O_3 measurements. In order to

provide an estimate of the atmospheric O_3 distribution across this altitude gap region, the in situ measurement made on board the DC-8 was used in fitting a third degree polynomial between the nearest 1 km of DIAL O_3 data in the nadir and zenith directions. To avoid introducing anomalous values of O_3 in cases where the near-field DIAL data exhibited a steep O_3 gradient, such as when the aircraft was near the tropopause, a constraining O_3 point was introduced into the altitude gap midway in value and position between the in situ measurement and the nearest DIAL measurement in the nadir and zenith directions before the fit was preformed. If the vertical gap between the aircraft and the start of the DIAL data exceeded 3.5 km, no fit was attempted, and this occurred very infrequently.

An estimate of the atmospheric O_3 distribution below the lowest DIAL measurement to just above the surface was determined from the DC-8 in situ O_3 measurements. Empirical relationships between in situ O_3 measurements just above the surface (generally ~300 m) and 1.5 km, and 1.5 and 3.0 km were derived for each flight. These ratios were then used to piecewise linearly extrapolate the DIAL data from the lowest DIAL measurement to the surface. No vertical extrapolation was done if the DIAL data did not extend down below 3 km above the surface, as often was the case when convective clouds were present. Most of the DIAL measurements outside of clouds extend to below 2 km. Horizontal gaps in the extrapolated O_3 fields are filled in using a linear least squares interpolation of remote and in situ data for data gaps of less than 30 min.

Since this is a tropospheric investigation, the DIAL data collected above the tropopause are removed from inclusion in this study. The method for determining tropopause height from the DIAL O_3 data is described by *Browell et al.* [1996b]. Briefly, this
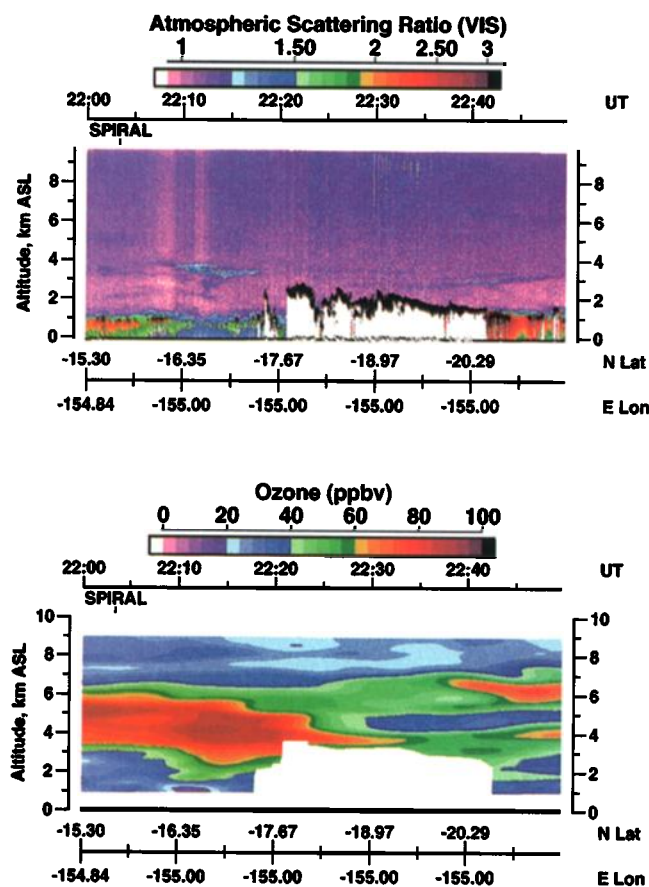
Atmospheric Scattering Ratio (VIS)

Ozone (ppbv)

Plate 1. Nadir DIAL O_3 and aerosol cross sections from PEM-Tropics A flight 6, September 5, 1996. From 2115 to 2140 universal time (UT), lidar signal attenuation resulting from cloud interference results in missing data below the cloud tops. Latitude in fractional degrees north (N Lat) and longitude in fractional degrees east (E Lon) are given on the scales below the images; UT is given on the scales above the images. The O_3 mixing ratio in parts per billion by volume (ppbv) is defined by the color scale at the top. Black represents values greater than 100 ppbv. The altitude scale is geometric altitude above sea level (asl). Aerosol data are visible scattering ratios plotted on a logarithmic scale.

technique involved determining the altitude of the intersection of a linear fit to the O_3 gradient in the lowest region of the stratosphere (region of 150–400 ppbv O_3) with the average O_3 level in the upper troposphere. After elimination of the stratospheric O_3 data, the resulting O_3 field represents our best estimate of the tropospheric O_3 distribution for each flight. An example is shown in Plate 2 with the interpolated and extrapolated data shaded. Contour overlays of PV are also shown, and they will be discussed in sections 2.4, 3.3, and 3.5.

Since an equivalent in situ measurement of atmospheric backscattering is not available on the DC-8, we do not attempt to interpolate the atmospheric scattering measurements across the altitude gap around the aircraft, nor do we attempt to correct for highly attenuated regions on the far side of clouds.

2.3. Other Airborne Measurements

The DC-8 had instrumentation for in situ measurements of O_3, aerosols, and nonmethane hydrocarbons (NMHCs) [Blake et al., this issue]; nitrogen dioxide (NO_2) and nitric oxide (NO)

(J. Bradshaw et al., unpublished manuscript, 1998); carbon monoxide (CO) and methane(CH_4); hydrogen peroxide (H_2O_2) [O'Sullivan et al., 1999]; sulfur dioxide (SO_2) and dimethyl sulfate (DMS) [Thornton et al., 1999]; SO_4 and peroxyacetyl nitrate (PAN); [7]Be [Dibb et al., 1999]; nitric acid (HNO_3) [Talbot et al., 1999]; carbon dioxide (CO_2) [Vay et al., 1999]; other trace species and meteorological parameters such as temperature, dew point, and winds. A general description of these systems and their measurements is given by Hoell et al. [1999].

2.4. PV Measurements

PV is obtained from the ECMWF model data products which are derived from radiosonde and satellite data. The observational network in the South Pacific has about a 10°grid spacing [Godfrey et al., 1998]. The model products have a horizontal resolution of 2.5° (280 km) in longitude and 2.0° (220 km at the equator) in latitude. The vertical values are associated with 18 pressure levels from 1000 to 0.4 mbar. In the tropical troposphere, there are 11 levels up to 70 mbar (18.4 km), with vertical intervals varying from 1.2 to 2.5 with a mean of 1.84 km. As a result, the spatial resolution of the PV model data products is much coarser than the resolution of the UV DIAL O3 data (70 km horizontally and 300 m vertically).

There have been a number of studies in the past investigating the linkage between PV and O_3 in the troposphere for air masses originating in the stratosphere. The UV DIAL measured a stratospheric fold event in 1984 that was well-described by the associated PV field [Browell et al., 1987]. We have used PV cross sections in conjunction with DIAL O_3 data from PEM-West A [Browell et al., 1996a], PEM-West B (unpublished data), and TRACE A [Browell et al., 1996b] to verify that O_3 and PV correspond well in regions of stratospheric intrusions and in measurements on the lower stratosphere. Newell et al. [1997] compared average tropospheric O_3 and PV latitudinal cross sections over the western Pacific Ocean along the 140°E meridian for the PEM-West A and PEM-West B data sets, showing that general features found in O_3 cross sections are also found in the PV cross sections. They explain that both O_3 and PV have their source in the stratosphere and are both destroyed in the boundary layer. They point out that the ratio of PV to O_3 decreases with altitude in the troposphere due to the mixing with tropospheric air containing O_3 that was photochemically produced.

3. Approach for Air Mass Characterization

3.1. Use of Ozone and Aerosols for Discrimination of Air Mass Types

In order to estimate when a strong localized signal was present of either an O_3 enhancement from a stratospheric source or a tropospheric photochemical source, or an O_3 deficit from photochemically O_3 depleted air, we established a reference O_3 profile to which we would make comparisons of local variations in O_3. The reference profile, shown in Figure 3, was chosen to maximize the sensitivity to discrimination of air with elevated O_3 and of air with low O_3. Above 5 km, the O_3 reference profile is identical to that used in PEM-West and was originally derived from average O_3 data from PEM-West A [Browell et al., 1996a]. O_3 varies linearly from 40 ppbv at 5 km to 66 ppbv at 18 km. From the surface to 5 km, the reference profile is slightly higher than that used in PEM-West A, linearly decreasing to 25 ppbv at 1 km altitude. In this altitude range, the reference O_3 profile is similar to the median value of in situ O_3 measurements when the
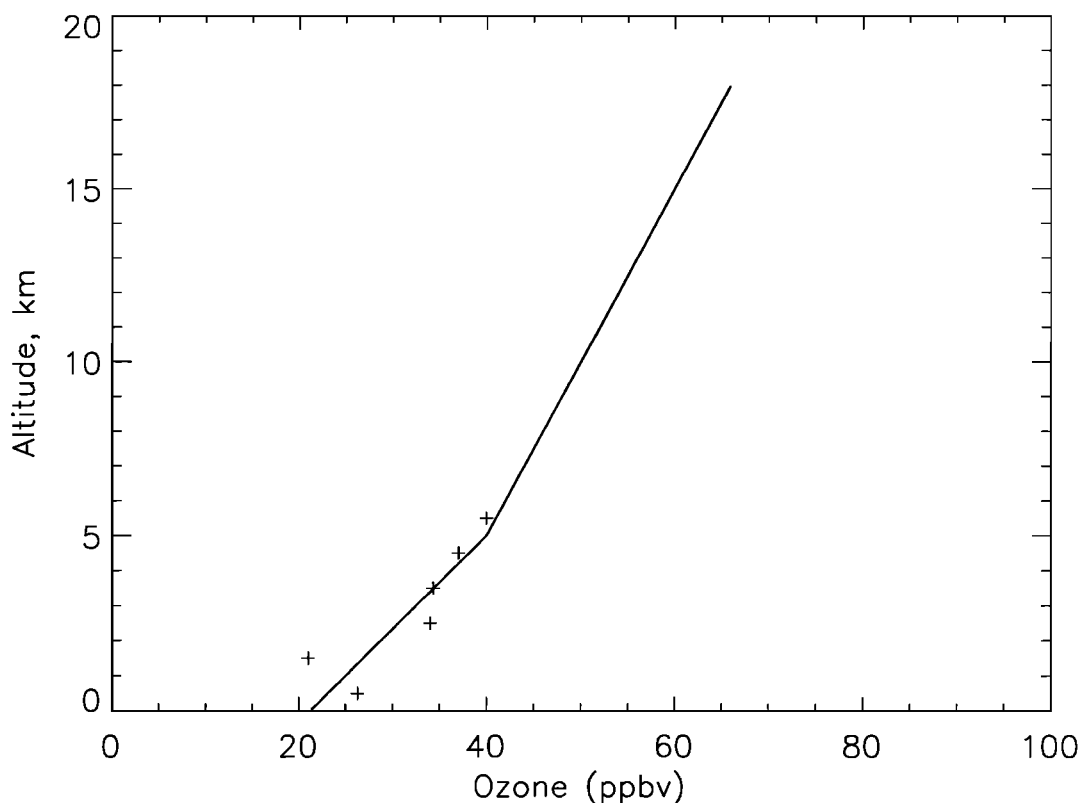
Figure 3. Reference O_3 profile used in air mass characterization analysis. Above 5 km, the same reference profile was used in similar analyses for PEM-West A and PEM-West B. Below 5 km, the PEM-Tropics A profile falls between the other two profiles. The median values of in situ ozone measurements accompanied by measurements of CO < 60 ppbv within the PEM-Tropics A air mass characterization study region are plotted as plusses for altitude bins of 1 km.

data were binned in 1-km intervals below 6 km and limited to relatively unpolluted cases where CO < 60 ppbv. Above 6 km, the unpolluted in situ O_3 measurements are considered to be biased low based on the available O_3 DIAL data in the mid to upper troposphere, and as a result, the in situ measurements were not used in developing the reference profile.

Aerosol scattering ratio data accompanying the DIAL O_3 data are also used in the air mass characterization. The air mass characterization studies done for PEM-West A [Browell et al., 1996a], PEM-West B [Fenn et al., 1997], and TRACE A [Browell et al., 1996b] found the aerosol data useful in further discriminating the relative age and origin of the air containing elevated O_3. Fresh biomass burning plumes in the lower and midtroposphere were heavily laden with aerosols in these studies. In addition, the eruption of Mount Pinatubo in 1991 provided significant stratospheric aerosol loading detectable in stratospheric intrusions in the upper troposphere. In PEM-Tropics A, aerosols and soluble ions had been largely washed out of the troposphere [Dibb et al., 1999], and the stratospheric aerosol loading was quite low as well. This made it difficult to remotely differentiate between elevated O_3 originating from photochemical production in the troposphere and elevated O_3 originating from transport from the stratosphere. Browell et al. [1996b] report examples from TRACE A of photochemically produced O_3 in air with no significant enhancement in aerosol loading with the air having been through a wet convective event. Still, occasional plumes with high aerosol loading and enhanced O_3 levels were observed in the western Pacific, and their distinct classification reflects that,

as described in section 3.4. The high aerosol loading just above the surface is used to identify the boundary layer.

3.2. Use of PV for Further Discrimination of Elevated Ozone Air

The lack of discriminating aerosol characteristics during PEM-Tropics A between stratospheric air and air from biomass burning regions that have had aerosols removed during convective transport forced us to investigate the relationship between PV and O_3 in the study region. In situ chemical measurements allowed us to use the full chemical signature of air parcels to identify 17 cases where air with elevated O_3 appeared to have a stratospheric component. The chemical signature we looked for was an enhancement in O_3 accompanied by a drop in CO and NMHC relative to the surrounding air. The PV for each of the 17 cases was determined from the ECMWF analysis, and a least squares linear relationship between O_3 and PV was fit to the data with a resulting slope of 4.2 ppbv/(10^{-7} deg K m^2 kg^{-1} s^{-1}) (Figure 4). We used this average slope and the PV associated with the remotely measured air having significantly elevated O_3 to estimate the amount of stratospheric O_3 that is in that air mass.

An example of one of the 17 cases occurred in flight 8, and it is shown in Plate 2. At the spiral point near 1500 UT, from 2–4 km O_3 averaged 48 ppbv; CO averaged 81 ppbv; and C_2H_6 averaged 452 pptv. For air perturbed by biomass burning sources in this altitude region, Blake et al. [this issue] report means and standard deviations of O_3, 60±14 ppbv; CO, 85±9 ppbv; and C_2H_6,
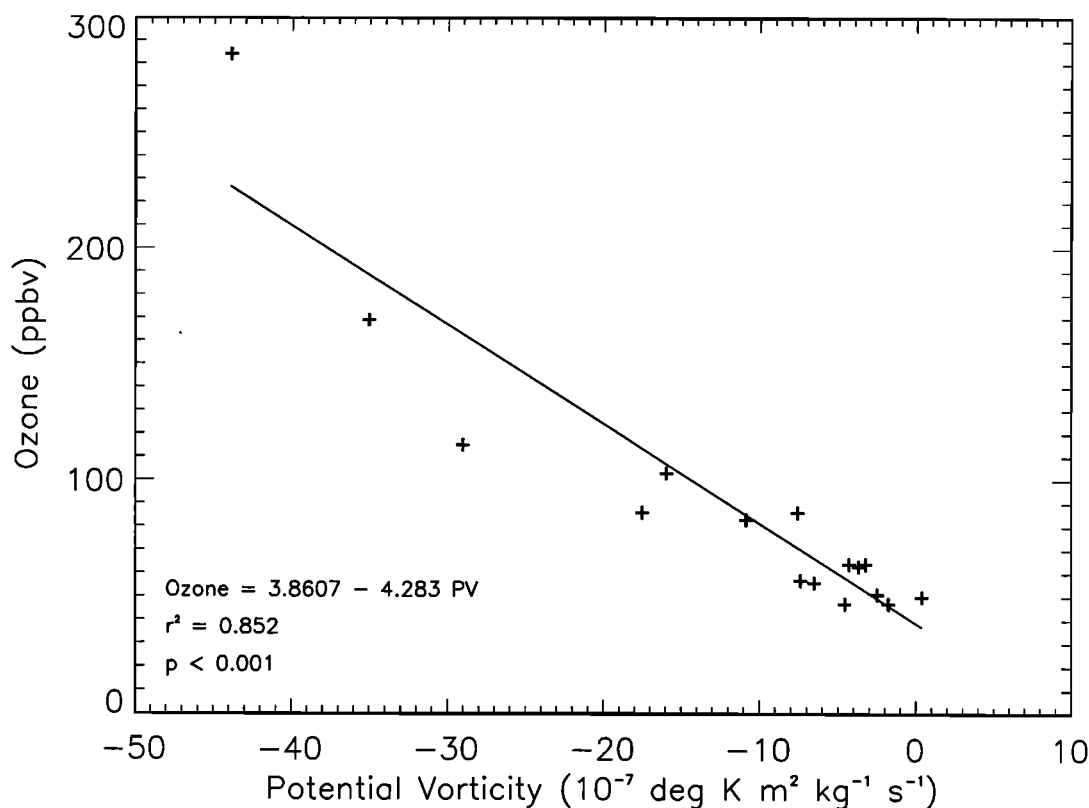
Figure 4. O_3 versus PV for 17 cases where in situ chemistry indicates some stratospheric contribution to the air.

465±146 parts per trillion by volume (pptv), and for unperturbed air they also report averages of O_3, 34±9 ppbv; CO, 52±2 ppbv; and C_2H_6, 295±38 pptv. Thus the air sampled on flight 8 from 2–4 km at the spiral point shows a definite impact of biomass burning. Later, the aircraft made measurements from 1645 to 1721 UT at 3.5 km from latitude 13.8°S to 16.2°S. This geographic location was overflown on the outbound leg from 1400–1418 as shown in Plate 2. At the start of the 3.5 km altitude leg, CO averaged 77 ppbv, and C_2H_6 was 464 pptv. After 3 min, CO dropped to values varying from 52–63 ppbv, C_2H_6 dropped to 344 pptv, yet the in situ O_3 remained elevated at 51 ppbv. The CO and NMHC measurements on this leg past the first 3 min do not suggest a biomass burning source for the elevated O_3. However, they do support a stratospheric component, as the relative humidity dropped from 12% to an average of 2.6%, and CH_4 dropped from 1723 ppbv to 1698 ppbv. The in situ measurement value of [7]Be over the entire 3.5 km leg was also elevated at 943 fCi/scm.

Back trajectory analyses also support the conclusion that this air contains a significant stratospheric component. Ten-day back trajectories were calculated from end points at latitudes 11.9°S, 14.9°S, 16.1°S, and 17.4°S along the 110°W meridian and at altitudes of 3.1 and 4.6 km. These geographic locations are annotated BT on Plate 2. At 4.6 km, all back trajectories indicated the air remained over the marine environment, staying north of 31°S latitude. At 3.1 km, the trajectory ending at 11.9°S remained between 4°S and 21°S latitude, coming from just off the western coast of South America. The back trajectories from 14.9°S, 16.1°S, and 17.4°S at 3.1 km had a different history with the air descending from above 10 km at latitudes south of 48°S. Figure 5 shows the PV cross section along the 107°W meridian at midnight on September 7, 1996. At that time, the air parcel which arrived

at 14.9°S at 3.1 km was at (23.5°S, 107.5°W) at 7 km. Figure 5 indicates that air parcel was part of a stratospheric intrusion. The PV contours overlain on the O_3 data in Plate 2 show a relative enhancement in PV on the 3.5 km leg south of ~13°S. We calculate the stratospheric contribution on this leg to be at lease 23–27% of the measured O_3. Nonexact spatial correlation between PV and O_3 fields usually result in an underestimate of the stratospheric contribution in the enhanced-O_3 air masses.

3.3. Description of All Air Mass Categories

A total of nine separate air mass types are defined in this study and summarized in Table 1. They depend on the deviation of the O_3 level in comparison to the reference profile, the aerosol loading, and the PV levels. The O_3 reference profile (Figure 3) is used to separate the troposphere into elevated-O_3 air, reference-O_3 air, and low-O_3 air. Enhanced aerosol loading is used to identify aerosol plumes and air associated with the boundary layer. Further discrimination of elevated-O_3 air in an attempt to differentiate various O_3 source regions relies on an estimate of the percentage of O_3 in the air that can be attributed to the stratosphere through the amount of PV that is present.

3.4. Case Study

Plate 3 displays the results of the air mass characterization applied to flight 8 (see the O_3 and PV in Plate 2). The only region of elevated aerosol loading is in association with the boundary layer and is categorized as near surface air (NS). There are no occurrences of high O_3 plume (HPLU) or background O_3 plume (BPLU) in this flight. Since the low-O_3 air is found without associated cirrus clouds, it is categorized as clean pacific (CP) rather than convective outflow (CON). The remaining air has
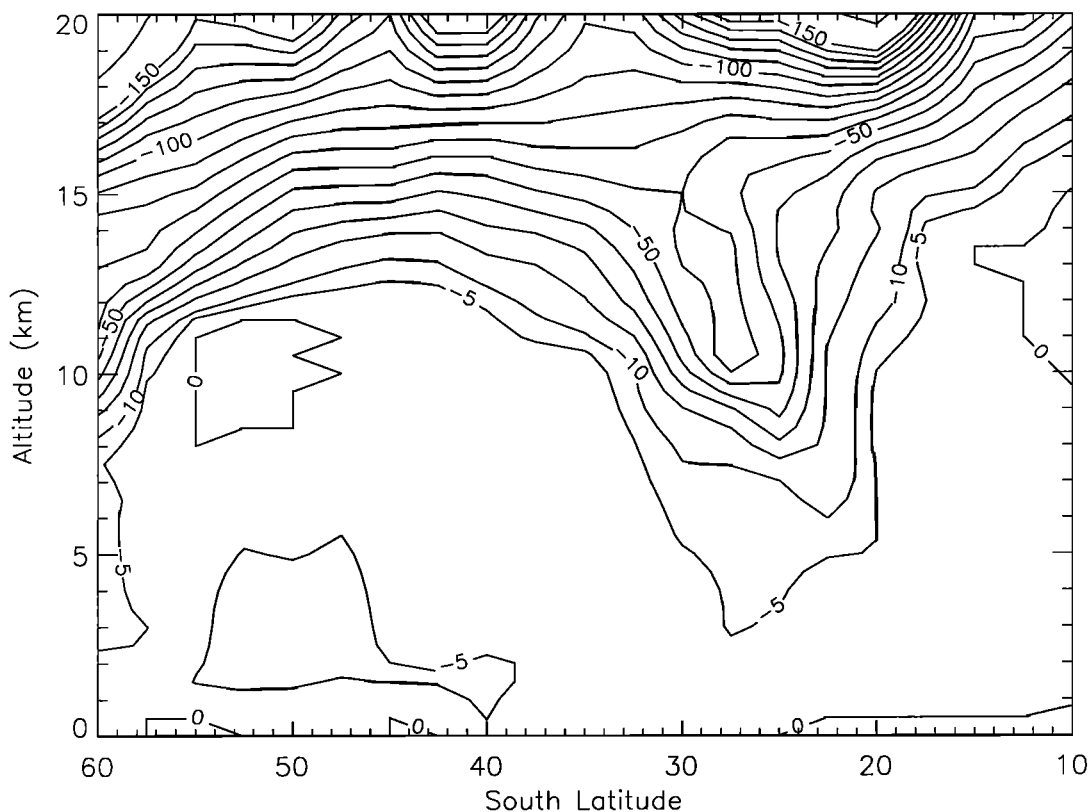
Figure 5. PV distribution along the 107 W meridian from ECMWF analysis of September 7, 1996. PV isopleths are in units of 10^{-7} deg K m^2 kg^{-1} s^{-1}.

elevated O$_3$, and the categorization depends on the relative amount of PV associated with it.

The PV field accompanying the elevated O$_3$ on flight 8 (see Plate 2) has many interesting features. Positive values of PV occur in the upper troposphere of the northern portion of the flight indicating this air has a northern hemisphere origin. Backward trajectories indicate that the air at 10 km came from near Central America just 4 days earlier [*Fuelberg et al.*, 1999]. *Blake et al.* [this issue] determined from the NMHC data that the source of the O$_3$ precursors in this air mass was not biomass burning, but natural gas and liquified petroleum gas (LPG) leakage. This air was categorized as HO3 (see Plate 3). Elsewhere on the flight, the PV is negative, indicating a southern hemispheric origin of the air. This is consistent with the meteorology of the region described in detail by *Fuelberg et al.* [1999], which indicates a westerly flow of air. The calculated stratospheric component to the elevated-O$_3$ air along the 3.5 km leg at 15°S is only sufficient to place it in the HO3M category (described in section 3.3). The HO3M category was also found just below the tropopause on the entire flight and in the midtroposphere at the southern end of the flight track. *Fuelberg et al.* [1999] suggest that a broad downward undulation in the tropopause occurs at the southern end of the fight track, consistent with enhanced PV above 9 km. As the PV increases at this location, the categorization changes from HO3M to SINF.

4. Discussion

4.1. PV and Ozone Characteristics of Air Masses

The tropospheric O$_3$ cross sections collected south of 10°N latitude during PEM-Tropics A were characterized using the

method described in section 3. The average vertical profiles of O$_3$ and PV for each air mass type are shown in Plate 4.

The average O$_3$ profiles of NS and reference-O$_3$ air shown in Plate 4a reflect the vertical profile of the reference profile (Figure 3). Low-O$_3$ air mass types contain an average of 32% of the O$_3$ mixing ratio found in reference air. The O$_3$ profiles of the air mass types having elevated O$_3$ indicate that the HO3 and HPLU types have similar enhancement in O$_3$ at altitudes less than 7 km, which is much higher than HO3M and SINF. SINF was observed below 7 km on only one flight (flight 13), whereas HO3M was observed below 7 km on 13 flights throughout the region.

Categorization of low-O$_3$, NS, and reference-O$_3$ air is independent of PV. Plate 4b indicates that there is still some residual PV even in these air mass types, with CON and CP having the lowest levels of PV. REF and HO3 have low values of PV ($\leq 2 \times 10^{-7}$ deg K m^2 kg^{-1} s^{-1}) below 8 km, and as expected due to the increase of O$_3$ with altitude for the reference profile, the average PV level for these categories increases to about 3 between 10 to 15 km. The increase of PV for REF above 14 km and CON and CP above 13 km is most certainly due to a mismatch in the spatial resolution of PV and O$_3$ in the vicinity of the tropopause where their gradients are large. PV in this altitude region is calculated only at 150, 100, and 70 mbar, corresponding to altitudes around 13.7, 16.2, and 18.4 km, while the vertical resolution of the O$_3$ data is 300 m.

Elevated-O$_3$ air relies on PV for categorization into HO3, HO3M, or SINF. A mismatch in PV in the vicinity of the tropopause could result in the identification of the air as HO3M instead of HO3. The PV of REF is more similar to HO3M than

Table 1. Definitions of Air Mass Types

Type	Definition
	Reference-O_3 Air
REF	air having O_3 values within 20% of the reference profile in the absence of enchanced aerosol loading
BPLU	air having O_3 values within 20% of the reference profile accompanied by appreciable aerosol loading
	Low-O_3 Air
CON/CP	O_3 values less than 20% lower than the reference profile. Convective outflow is assigned when clouds are also present in the area. Clean Pacific is assigned in the absence of cloud activity in the area.
	Elevated-O_3 Air
HPLU	air having O_3 values in excess of 20% greater than the reference profile accompanied by appreciable aerosol loading
HO3	air having O_3 values in excess of 20% greater than the reference profile and the fraction of ozone attributed to a stratospheric source being less than 20%
HO3M	air having O_3 values in excess of 20% greater than the reference profile and the fraction of ozone attributed to a stratospheric source being between 20% and 60%
SINF	air having O_3 values in excess of 20% greater than the reference profile and the fraction of ozone attributed to a stratospheric source being greater than 60%
	Other
NS	air having high aerosol loading associated with the boundary layer

REF, reference; BPLU, background O_3 plumes; CON/CP, convective outflow/clean Pacific; HPLU, high O_3 plumes; HO3, high O_3; HO3M, high O_3 mixed; SINF, stratospherically influenced; NS, near surface.

HO3 above 16 km which suggests such a mismatch might have resulted in an underestimate of HO3 at those altitudes (Plate 4b).

4.2. Geographic Distribution of Air Masses

The study region was divided geographically to investigate variations in the frequency of occurrence of the various air mass types (Figure 1). Table 2 summarizes the amount of the air mass types observed in each region over the entire troposphere. Many of the features of this distribution can be understood from the meteorological conditions that were present during the study period.

At low latitudes, *Fuelberg et al.* [1999] showed that the location of the Intertropical Convergence Zone (ITCZ) and South Pacific Convergence Zone (SPCZ) was located across the regions of the WPLL and CPLL. These zones are associated with widespread ascent and deep convection, and this accounts for the maximum amount of CON/CP in the WPLL and CPLL. The amount of total elevated-O_3 air is least in the low latitude regions,

reflecting destruction of O_3 in the marine boundary layer and convection to higher altitudes [*Thompson et al.*, 1993].

At midlatitudes, *Fuelberg et al.* [1999] reported that the mean airflow is from the west, following subsidence over Australia. Another area of subsidence occurs in EPLL and EPML. This explains the much smaller percentage of CON/CP in the WPML, WPHL, and EPML, as well as the large percentage of HO3M and SINF in these regions, as discussed below.

Air in the middle and lower troposphere arrives from the west at midlatitudes after having traveled from South America or Africa via upper tropospheric high winds [*Fuelberg et al.*, 1999; *Board et al.*, this issue]. Burning in southern Africa and South America is known to occur at this time of year, and is well documented by the Southern African Fire-Atmosphere Research Initiative/Transport and Atmospheric Chemistry Near the Equatorial Atlantic (SAFARI/TRACE A) experiments [*Cahoon et al.*, 1992] (SAFARI/TRACE A special issue of Journal of Geophysical Research, 1996). In particular, *Browell et al.*

Table 2. Percentage of Troposphere With Different Air Masses

Air Mass Type	WPLL	WPML	WPHL	CPLL	CPML	EPLL	EPML
REF	34.3	10.2	32.6	33.7	24.3	43.5	37.9
CON/CP	29.8	2.7	11.8	33.4	17.0	22.3	12.8
SINF	0.2	18.2	18.3	1.2	13.2	2.0	11.4
HPLU	0.0	8.6	7.6	0.0	0.0	0.0	0.0
HO3	19.0	27.9	7.0	16.3	27.8	13.9	13.5
HO3M	9.7	25.7	20.3	10.5	12.8	14.3	21.4
Total elevated O_3	28.9	80.4	53.2	28.0	53.8	30.2	46.3
NS	6.9	6.4	1.7	5.0	4.8	4.0	2.9
NS (1-3 km)	55.0	45.0	9.3	39.9	33.6	32.4	20.5
BPLU	0.0	0.3	0.8	0.0	0.0	0.0	0.0

Ozone (ppbv)
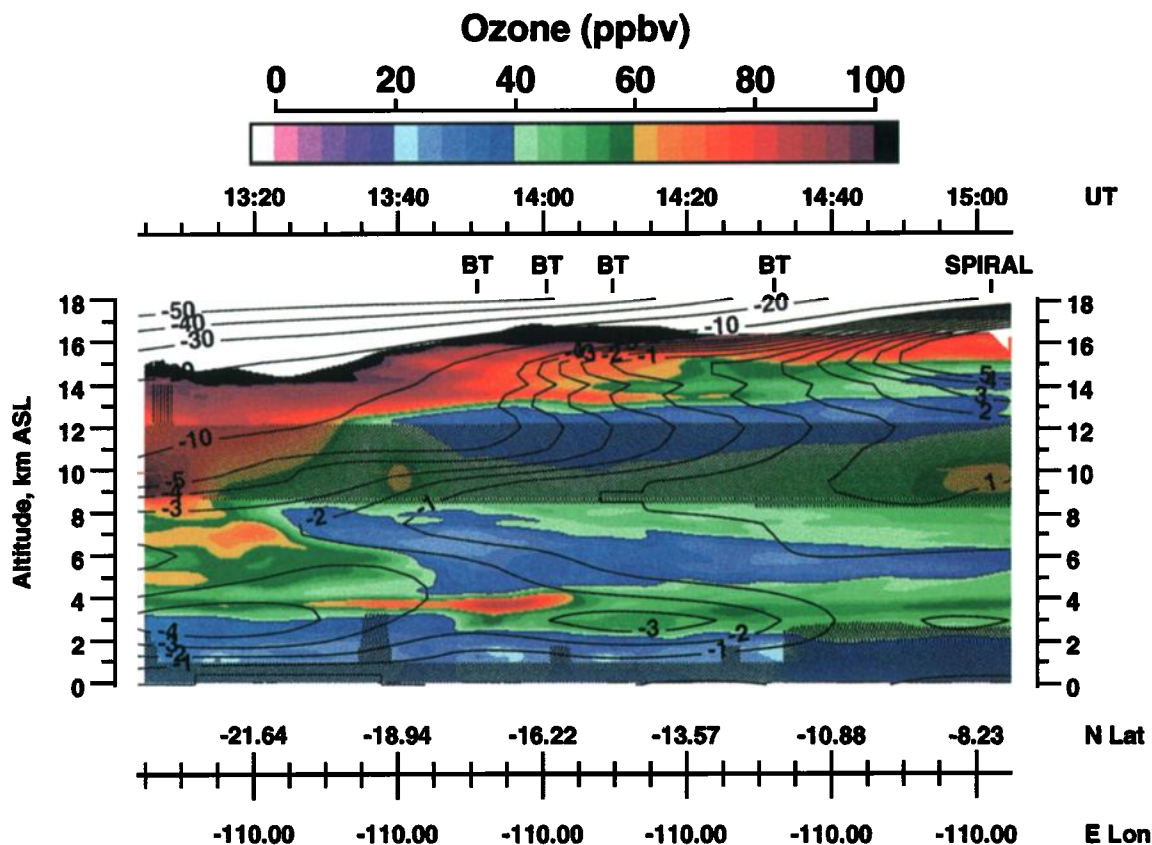
Plate 2. Tropospheric O_3 distribution for PEM-Tropics A flight 8, September 10, 1996, including interpolated and extrapolated O_3 estimates in shaded regions. Isopleths of PV distribution along the DC-8 flight track from ECMWF analysis of September 10, 1996, are overplotted in units of 10^{-7} deg K m^2 kg^{-1} s^{-1}.

Air Mass Characterization
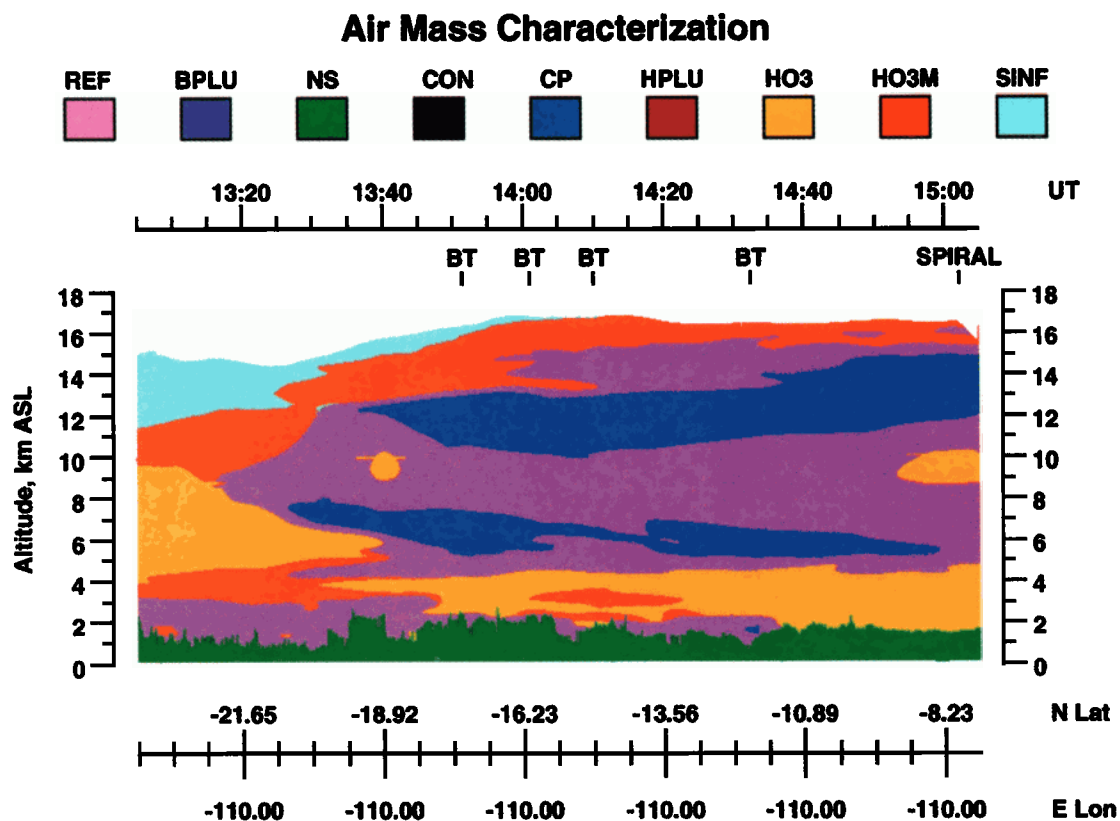
Plate 3. Air mass identification of troposphere for flight 8. Back trajectory calculations occurred at locations marked with "BT." Codes for various air mass types are defined in Table 1.
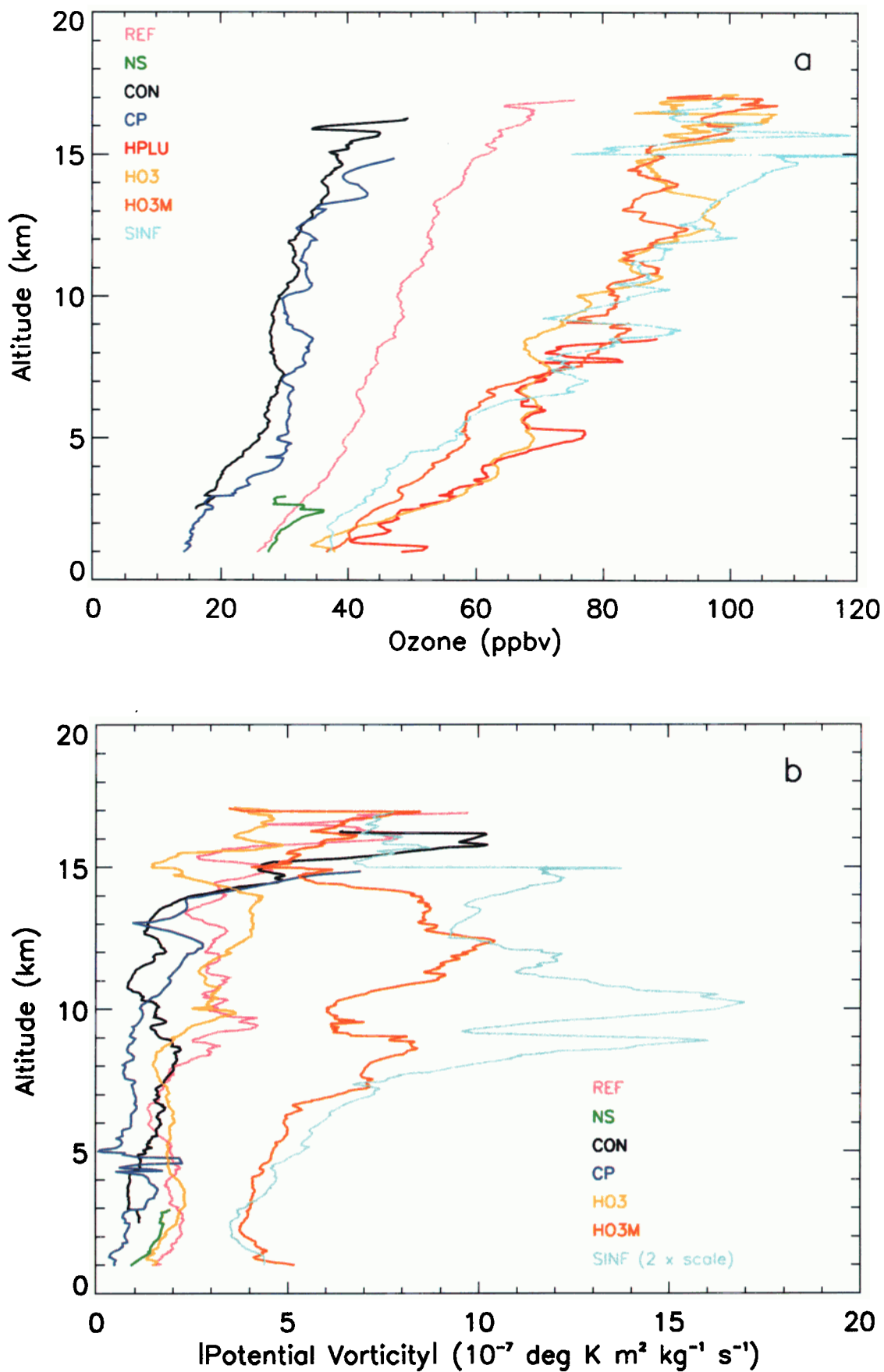
Plate 4. (a) Vertical profiles of mean O_3 for each air mass type in the study region. (b) Vertical profiles of mean absolute value of PV for each air mass type in the study region.
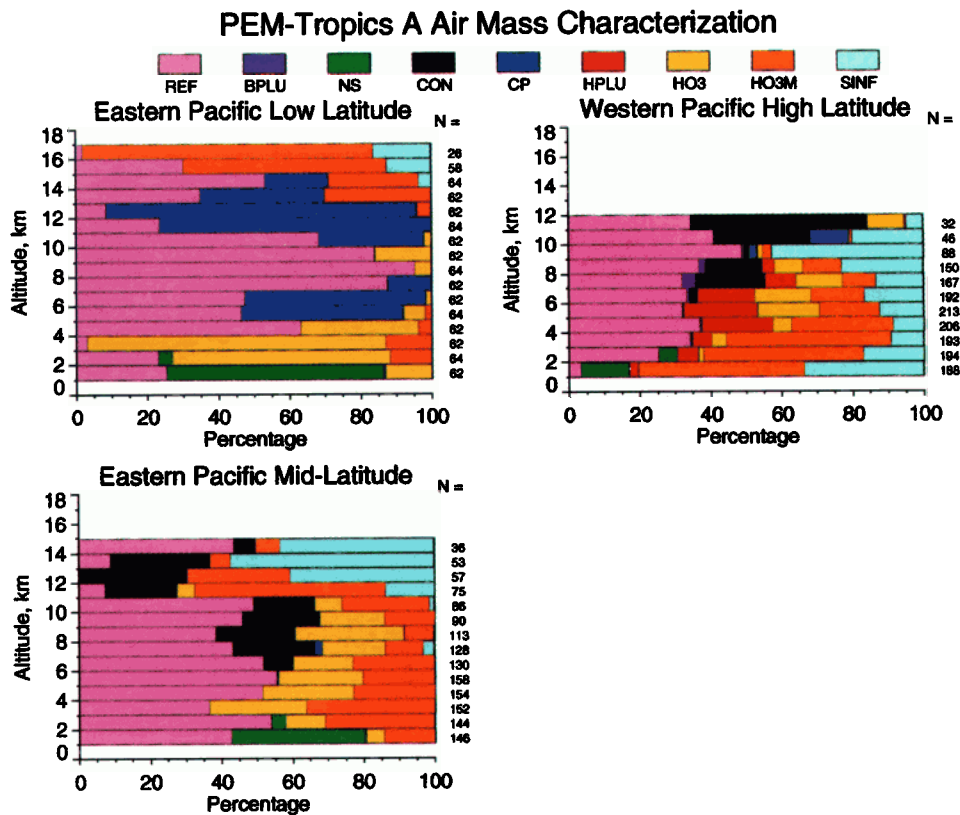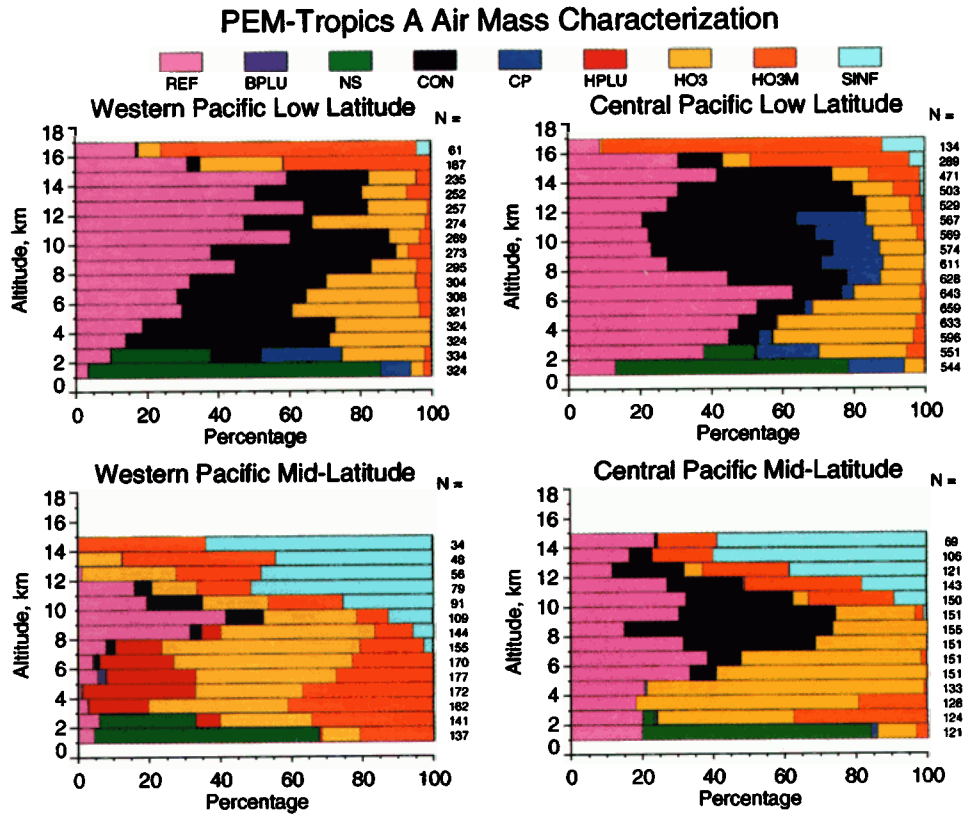
Plate 5. Percentage of observations of different air masses over the subregions of the PEM-Tropics A region. The number of independent samples included in each 1-km altitude bin is given at the right of each graph.

[1996b] measured elevated O_3 of biomass burning origin throughout the troposphere at the same time of year over South America and southern Africa. In the upper troposphere, tropospheric air can pick up O_3 and PV by mixing with air in the vicinity of the tropopause before subsiding over Australia and being advected across the Pacific. This air contains elevated O_3 precursors of biomass burning origin [*Talbot et al.*, 1999; *Blake et al.*, this issue; *Board et al.*, this issue], and the biomass burning plumes become diluted as they cross the Pacific [*Schultz et al.*, 1999]. The enhanced PV associated with this air reflects its transport history in the upper troposphere. The amount of HO3 is nearly the same in the WPML and CPML regions, but it decreases abruptly to the east in the EPML region. There is a slight decrease in SINF at midlatitudes from west to east, but the amount of HO3M is nearly as large in EPML as in WPML, both regions of subsidence. While the percentage of SINF increases drastically from low to midlatitudes due to the lowering of the tropopause height at higher latitudes and the proximity to the subtropical jet at ~30°S, the amount of SINF was nearly the same between the mid and high latitudes in the western Pacific.

Aerosol-laden plumes, identified as mainly HPLU, occurred mostly below 9 km, and as far south as 52°S. They were identified only in the WPML and WPHL regions where they make up 13 and 11%, respectively, of the air from 1–9 km. These regions of the study area were most directly affected by air in recent contact with land. Aerosol loading in these plumes was high since they had been advected directly from the biomass burning regions with little or no washout from cloud convection.

The frequency of observation of the different air mass types was calculated from 1 km to 17 km in 1-km increments, and the results are reported when the number of independent samples (300 m vertically and 70 km horizontally) in an altitude bin exceeds 20 (Plate 5). Air with elevated O_3 was observed throughout the troposphere in every region except in the middle troposphere of the EPLL, where limited sampling may have biased the observations. In general, the amount of elevated-O_3 air having some stratospheric component (HO3M plus SINF) increased with altitude. REF was also present at all altitudes, but CON/CP was more common in the middle to upper troposphere,
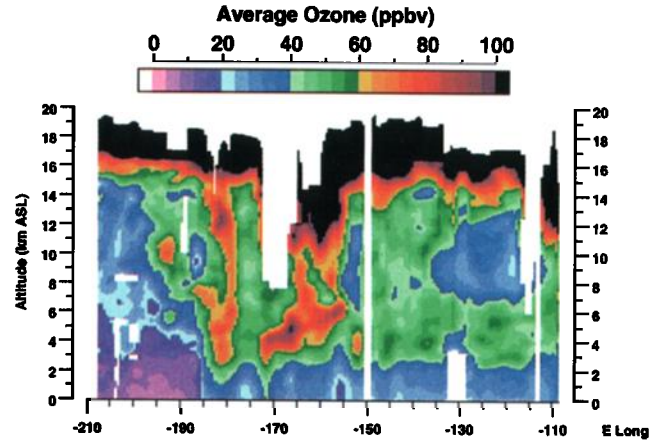
Plate 7. Average O_3 distribution from 30°S to the equator across the study region. Data are included from complete tropospheric cross sections.

except in the WPLL where it occurred at all altitudes due to cloud pumping associated with the ITCZ and SPCZ. As expected, NS is only present below 3 km since boundary layer depths did not exceed that altitude. The percentage of NS air above 1 km increased at the lower latitudes as boundary layer development was enhanced over the warmer water. Table 2 includes the percentage of NS air from 1–3 km as well as over the entire troposphere.

A significant amount of HO3 was found below 16 km in WPLL and CPLL. Very little HO3M air was present in these regions below 14 km. *Board et al.* [this issue] used back trajectory calculations at the aircraft altitude (less than 12.5 km) to show that air parcels in these regions arrived from Australia and Southeast Asia by way of Australia containing a weak biomass burning signature. They report these air masses travel shorter distances, and many are at lower altitudes, than those coming from South America or Africa. They also report finding indications of NO from lightening. The amount of HO3 found above 16 km may be underestimated as mentioned in section 4.1.

In the regions of subsidence, WPML, WPHL, and EPML, the amount of elevated-O_3 air having a stratospheric component (SINF and HO3M) was significant throughout the troposphere. *Board et al.* [this issue] restricted their back trajectory analyses to arrivals north of 35°S, and for the WPML and EPML, they reported air arriving from Africa and South America traveling at high altitudes. These air masses could have been mixed in the upper troposphere with air having a stratospheric origin, and this would have resulted in a weak to moderate PV signature as well as a biomass burning signature.

HO3 in the midlatitudes occurs predominantly at altitudes below 11 km. *Board et al.* [this issue] reported that air with a moderate biomass burning signature arrived in this region from Australia, after having traveled shorter distances and at lower altitudes than those trajectories coming from Africa or South America. As a result, this air would have less accompanying PV. *Olson et al.* [1999] shows that burning was occurring on the east coast of Australia during PEM-Tropics A.

4.3. Average Ozone Distributions

The average O_3 distributions observed during PEM-Tropics A were obtained by binning the derived O_3 cross sections (DIAL O_3 plus extrapolated and interpolated O_3 estimates) for each flight
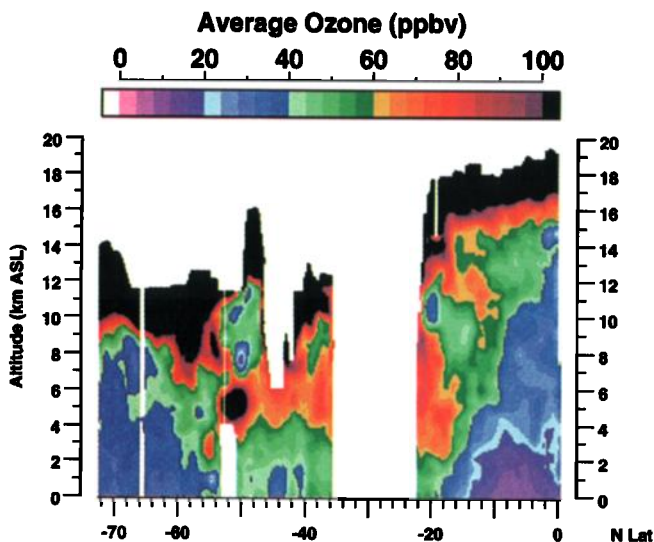

Plate 6. Average O_3 distribution across the western South Pacific. Data are included from complete tropospheric cross sections on flights west of 170°W longitude.

Table 3. Air Mass Composition (Average Value/Median Value (Number of Cases))

	Air Mass Type (Number of Cases)						
	REF (29)	NS (16)	HPLU(4)	SINF(5)	HO3M(13)	HO3(35)	CON/CP(31)
Geometric altitude, km	8.0/8.2	0.6/0.5	6.3/6.8	8.1/9.1	7.4/7.1	5.8/5.8	8.4/9.3
Relative humidity, %	32.0/20.9	80.2/82.0	47.4/72.2	14.4/14.7	22.7/17.4 (12)	12.9/8.4 (34)	33.8/29.2
O_3, ppbv	42.4/43.8	20.5/18.3	68.8/70.5	116.5/115.8	68.0/72.3	72.0/69.2(34)	28.4/29.6
CO, ppbv	62.3/60.2	58.3/54.5	126.2/139.7	54.5/58.3	70.9/66.4	82.0/80.0	55.8/56.0
CH_4, ppbv	1704.6/1704.4 (26)	1696.9/1697.8	1710.3/1710.6	1683.2/1683.2	1703.9/1701.5 (12)	1715.1/1714.1 (34)	1705.3/1707.2 (30)
SO_2, pptv	14.1/13.6	33.2/30.4	13.3/14.2(3)	13.4/10.5	14.0/14.3	13.4/12.1 (33)	21.5/16.4
DMS, pptv	1.9/1.5	55.7/56.4	1.5 (2)	2.1/2.0	1.8/1.5(12)	1.4/1.5 (31)	5.4/1.8(30)
PAN, pptv	44.5/41.0	3.0/1.1(15)	337.1/468.0	61.2/56.6	78.4/76.7	130.3/116.1	18.2/19.0(30)
C_2Cl_4, pptv*	1.28/1.27 (27)	1.40/1.35	1.61/1.70	0.65/0.70(3)	1.32/1.30(12)	1.39/1.33(31)	1.29/1.35(27)
NO, pptv	29.2/11.4(21)	2.2/1.4(13)	11.4/11.2	12.4/13.6	58.1/29.2(11)	23.2/17.9(29)	22.3/20.2(29)
NO_2, pptv	10.8/8.9 (14)	4.4/3.6(10)	11.8/12.9 (3)	8.4/5.6(4)	16.8/9.8(9)	24.0/23.8(20)	6.2/4.5(14)
CH_3CCl_3, pptv	83.3/83.4(27)	83.8/84.5(14)	81.9/82.2	78.6/79.1 (4)	82.8/83.1	83.5/83.6(34)	83.1/83.5(27)
C_2H_6, pptv	349.3/346.3(27)	295.1/307.7(14)	812.3/829.2	274.5/278.1	429.5/408.9	528.9/478.3(34)	284.4/280.1(27)
C_2H_4, pptv	2.18/2.08(27)	2.99/3.01 (14)	2.75/2.77	2.09/2.00	2.24/2.20	2.41/2.30 (34)	2.10/2.01 (27)
C_2H_2, pptv	52.5/43.8 (27)	36.8/39.0(14)	244.1/300.2	44.0/43.6	80.8/77.1	97.7/91.3(34)	31.2/31.2(27)
C_3H_8, pptv	26.4/21.3(27)	22.4/19.0(14)	54.0/51.0	17.1/15.9	29.5/28.8	38.4/29.4(34)	17.4/14.9(27)
Isobutane, pptv	2.1/2.0(27)	2.3/2.0(14)	3.1/3.0	2.0/2.0	2.0/2.0	2.3/2.0 (34)	2.0/2.0(27)
CH_3I, pptv	0.07/0.06(26)	0.34/0.37(14)	0.04/0.04	0.05/0.06	0.07/0.06	0.06/0.06 (34)	0.09/0.08(27)
CH_3Cl, pptv	563.1/562.2(27)	549.0/548.9(14)	599.5/606.7	547.6/550.0	571.7/569.5	577.8/576.5(34)	551.3/551.2(27)
CH_3Br, pptv	8.44/8.53(27)	8.10/8.14(14)	8.98/8.97	8.18/8.19	8.54.8.62	8.93/8.92 (34)	8.44/8.43(27)
$CHBr_3$, pptv	0.46/0.44(27)	1.25/1.29(14)	0.45/0.49	0.14/0.15(4)	0.38/0.32	0.38/0.37 (34)	0.58/0.58(27)
CO_2, ppmv	360.9/361.0(28)	361.0/361.3(14)	362.2/362.3	360.5/360.4	361.1/361.1	361.0/361.1	361.0/361.0
H_2O_2, pptv	423.0/378.5(28)	1012 /1192	1214.1/1604.1	83.2/89.8	380.0/286.7	737.4/644.6	468.3/328.6
CH_3OOH, pptv	267.1/229.1(28)	861.0/1012.0	418.2/565.8	90.5/73.1	219.5/186.3	242.3/190.9	318.4/210.5
Ultrafine aerosol, cm^{-3}	2737/1713(27)	392/353(14)	851/882	673/669	1886/1148	1274/909 (31)	2589/2527(25)
Unheated fine aerosol, cm^{-3}	1497/955(25)	275/245(14)	521/547	378/400	1052/693 (11)	698/507 (29)	1285.4/1343.1 (25)
Aerosol ratio	0.19/0.16(24)	0.25/0.23(13)	0.68/0.68	0.45/0.45 (4)	0.34/0.35 (4)	0.60/0.55 (27)	0.09/0.05(25)
Sulfate, pptv	26.2/18.0(10)	149.5/130.0(15)	211.3 (2)	31.1/36.2 (4)	25.1/27.6(4)	38.5/30.2 (10)	20.0/17.0(11)
Nitrate, pptv	31.2/19.0(5)	64.8/51.0(11)	74.1 (2)	27.0 (2)	48.0 (1)	65.5/58.0 (6)	45.4/37.0(9)
^7Be, fCi/scm	615.2/520.8(6)	337.0 (2)	255.0 (1)	2955/4326 (4)	1001/935 (5)	681.5/539.0 (12)	438.8/429.1(8)
^{210}Pb, fCi/scm	2.05/2.00(7)	1.88/1.70(9)	8.8 (1)	3.70/4.20 (4)	3.69/3.31(5)	5.29/4.28(13)	1.39/1.57(10)
HNO_3, pptv	65.8/57.7(25)	20.1/18.3(15)	223.3/293.4 (3)	274.1 (2)	86.9/63.2 (9)	192.2/164.1(13)	48.2/41.9(30)
CH_3COOH,pptv	48.9/43.0(24)	22.6/22.0(15)	317.3/352.3 (3)	48.8 (2)	80.6/54.2(9)	110.8/95.4(31)	40.1/34.3(29)
HCOOH, pptv	50.8/45.6(24)	22.0/18.2(15)	454.4/576.0 (3)	94.9 (2)	84.8/56.3 (9)	151.9/103.7(31)	35.2/34.1(29)
$C_2H_2/CO^\dagger$	0.81/0.78(27)	0.60/0.61(14)	1.81/2.02	0.76/0.75	1.09/1.13	1.14/1.15(34)	0.55/0.53(27)
C_3H_8/C_2H_6	0.073/0.077(27)	0.074/0.062(14)	0.067/0.067	0.059/0.062	0.069/0.067	0.067/0.060(34)	0.060/0.055(27)
O_3/CO	0.68/0.70 (28)	0.35/0.35	0.56/0.53	2.70/2.53	1.03/0.95	0.91/0.89(34)	0.51/0.51
$Sulfate/O_3^\dagger$	0.58/0.52(8)	8.12/8.10(14)	3.22 (2)	0.30/0.28(3)	0.34/0.27(5)	0.34/0.27(10)	0.62/0.53(10)
$NO_2/O_3^\dagger$	0.25/0.18(13)	0.28/0.36(10)	0.16/0.18 (3)	0.12/0.05(4)	0.24/0.16(9)	0.32/0.32(19)	0.22/0.18(14)
$^7Be/O_3$, (fCi/scm)/ppbv	13.2/10.4(8)	9.0 (2)	3.63 (1)	25.0/25.5(4)	12.5/12.0(5)	8.3/7.4 (13)	16.2/17.9(8)
Potential vorticity , 10^{-7} deg K $m^2 kg^{-1}s^{-1}$	−2.81/−2.04	−1.00/−0.10	−5.25/−3.54	−34.4/−30.9	−6.27/−4.90	−2.00/−2.00	−0.76/−0.78

*UC Irvine.
†Units in pptv/ppbv.

into 0.25° latitude and 0.5° longitude intervals. The binned O_3 data were averaged on a flight by flight basis, then those flight averages were combined. The method for this calculation is described in more detail by Browell et al. [1996b]. These calculations included both tropospheric and stratospheric O_3 data. Plate 6 shows the average O_3 latitudinal distribution for all flights west of 170°W longitude, corresponding to the WPLL, WPML, and WPHL regions. The data gap between 22°S and 35°S resulted from the lack of O_3 data in this region on flight 14. The altitude of the 100 ppbv contour decreased with increasing latitude, demonstrating changes in the tropopause height from about 17 km at the equator to below 10 km at high latitudes. The

broad region of air with O_3 in excess of 40 ppbv at altitudes from the surface to the tropopause and from latitudes 18°S to 51°S resulted from the long-range transport of high O_3 air from the west. Convective mixing of low O_3 air (<30 ppbv) throughout the troposphere is evident at low latitudes. Plate 5 shows that the majority of CON/CP was in the WPLL, and the majority of the elevated-O_3 air was in the WPML.

Plate 7 shows the average longitudinal O_3 cross section derived from all flights between the equator and 30°S. This corresponds to all the flights in the EPLL, CPLL, WPLL, CPML, and a portion of WPML and EPML. Note that WPML is not well represented because of lack of O_3 data on flight 14 north of 30°S. As a result, the average O_3 levels west of ~180° longitude are lower than they would have been if data from 22°S to 30°S had been included. Here the importance of CON/CP in WPLL is evident. East of ~180° longitude the enhanced tropospheric O_3 levels can be mainly explained by the HO3 air in the WPML and CPML. The proportion of HO3 and HO3M air masses decreases from west to east (Plate 5), while REF air increases in about the same proportion. This trend is reflected in the decreasing O_3 levels to the east of ~180° longitude (Plate 7).

4.4. Chemical Characteristics of Air Masses

A detailed chemical characterization of the various air mass types encountered during PEM-Tropics A was made using the comprehensive in situ measurements on the DC-8 [*Hoell et al.*, 1999]. Flights and time periods were identified that corresponded to cases where in situ sampling occurred within the various air mass types that were previously defined. It was not required that the DIAL system observe the same air remotely, since the interpolation technique provided a complete tropospheric cross section of O_3, and in this mission aerosol measurements were not crucial to the identification of the air mass since there were very few cases of enhanced aerosol loading above the boundary layer. As a result, the number of in situ cases available for chemical characterization increased by a factor of at least 3 for most of the categories compared to PEM-West A. Although BPLU was identified remotely by the DIAL system, in situ measurements are not available for this air mass type due to its limited spatial extent. Table 3 gives a summary of the combined chemical signatures of each of the air mass types based on the in situ sampled cases. Details about the locations of the in situ samples included in these averages can be found at the GTE web site.

Table 3 includes the mean and median values for the in situ measurements for each air mass type. NS air, which is defined as boundary layer air, was sampled below a maximum altitude of 2.4 km. The other air mass types were sampled through the full range of the troposphere accessible to the DC-8 from the top of the boundary layer to below 12.5 km. In general, the mean chemical composition of each air mass type was as expected. Combustion products, such as CO, NMHCs, PAN, peroxides, and HNO_3, HCOOH, and CH_3COOH had their highest concentrations in the HPLU category. So did tracers of continental influence such as ^{210}Pb and C_2Cl_4. Among the elevated-O_3 air mass types, mixing ratios of combustion products and continental tracers, as well as C_2H_2:CO decreased as expected in order HPLU, HO3, HO3M, and SINF. While recognizing that differences in source strengths and mixing processes during transport can influence measured values of C_2H_2:CO, *Board et al.* [this issue] used values of ~2 pptv/ppbv to represent air that is aged 2-3 days from its source region, and they used a value of ~0.5 pptv/ppbv to represent air that is aged approximately 10 days. This is

consistent with the idea that HPLU contained the freshest biomass burning output. HO3 was older air from a biomass burning source with aerosol washout from convection as indicated by low values of soluble gases such as the peroxides, and HO3M resulted from mixing in the upper troposphere of an HO3 air with air having some stratospheric component. The mean values of ^7Be decreasing from SINF to HO3M to HO3 is also as expected, since ^7Be has its primary source in the stratosphere [*Junge*, 1963].

The PV for each case was also calculated from ECMWF data. CON/CP has the lowest levels, followed by NS, and REF. As expected, the PV increases from HO3 to HO3M to SINF. HPLU has higher PV than HO3, perhaps because it occurs only in WPML and WPHL which are regions of subsidence.

As expected, the relative humidity was highest in NS, CON/CP, and HPLU air masses. NS had elevated peroxides and methyl iodide (CH_3I) with respect to REF air, while CON/CP had lower peroxides than NS air due to photochemistry and washout in convection. The ratio of C_2H_2:CO suggest that CON/CP was the oldest air mass types sampled.

Note that the ^7Be:O_3 was higher in CON/CP than in REF. Photochemical destruction of O_3 could have been responsible for increasing that ratio. Photochemical production of O_3 in HPLU and HO3 could have depressed ^7Be:O_3 in those categories.

O_3:CO clearly reflects the higher values associated with the stratospheric air component in SINF. This ratio is higher for HO3 and HO3M than for HPLU possibly as a result of more time for CO oxidation in an air mass with a longer lifetime [*Mauzerall et al.*, 1998]. The lowest values are found associated with the boundary layer and the oldest air masses in the free troposphere.

Blake et al. [this issue] report average values for unpolluted air from 0-12 km, defined as air having in situ CO < 55 ppbv. These values are most similar to those in the CON/CP category, having mean and standard deviation values of CO=51±4 ppbv, C_2H_6=287±48 pptv, C_2H_2=32±12 pptv, and C_3H_8=19±8 pptv.

Board et al. [this issue] report median chemical values for groups of air having a common geographic origin. Although their analysis is limited to a region north of 35°S and is not segregated by O_3 amount, their aged marine category is very similar in composition to the CON/CP reported in this paper. They report median values of O_3=34 pptv, CO=56 ppbv, C_2H_2:CO=0.56, HNO_3=52 pptv, HCOOH=37 pptv, CH_3COOH= 37 pptv, and ^{210}Pb=2.2 fCi/scm. Their long-range trajectory category from South America and Africa has CO=70 ppbv, C_2H_2:CO=1.1, ^7Be=1000 fCi/scm, NO=65 pptv, HCOOH=97 pptv, CH_3COOH=86 pptv, and ^{210}Pb=4.7 fCi/scm, which is similar in composition to HO3M. Their Australia category is most similar to HO3 with median values of CO=75 ppbv, C_2H_2:CO=1.1, HNO_3=180 pptv, HCOOH=147 pptv, CH_3COOH=91 pptv, and ^{210}Pb=5.3 fCi/scm.

4.5. Comparisons With Other Studies

Francey et al. [1999] reported on a series of instrumented flights over the Southern Ocean 35 km west of Cape Grim at 40.5°S, 144.3°E from 1992 to 1995. CO was found to be elevated in the 5-8 km region in the July-October time frame. *Komala et al.* [1996] reported enhanced O_3 observed in the middle and lower troposphere during September-October 1993 from ozonesondes launched from Watukosek, Indonesia, at 7.5°S, 112.6°E. *Kent et al.* [1998] reported Lidar In-Space Technology Experiment (LITE) and Stratospheric Aerosol and Gas Experiment II (SAGE II) aerosol data in the upper troposphere for the southern hemisphere. LITE flew on board the space shuttle on

September 10–20,1994. Aerosol layers were sometimes found in the 5–10 km region, with properties similar to aerosols measured during TRACE A by *Anderson et al.* [1996]. The SAGE II 6.5-km data show a band of aerosols around 25°S to 35°S in the September–November period, seeming to emanate from the Amazon Basin then drift over South Africa and the southern part of Australia. The 12.5-km data show an even larger extent of aerosols, from 10°S to 40°S, with South America, southern Africa, and Australia appearing to be source regions for the aerosols. Because of the limb-viewing nature of the satellite measurements, the sensitivity to aerosols is greatly enhanced over the direct lidar backscatter measurements discussed in this paper.

5. Conclusions

The troposphere over the South Pacific during the Southern Hemisphere burning season is influenced by a complex combination of different air mass types. The distribution of O_3 and aerosols, along with PV analyses, were used to differentiate between nine air mass types.

The average chemical composition of the nine air mass types was calculated from in situ chemical measurements and compared to the chemical composition of air divided by origin in back trajectory analyses reported by *Board et al.* [this issue]. The low-O_3 air is similar in composition to air that has been over the ocean for at least 10 days. Air with elevated O_3 and a moderate stratospheric component (over 20%) is similar in composition to air arriving from South America and southern Africa via upper tropospheric winds. The enhanced O_3 is due to both photochemical production of O_3 from biomass burning emissions and contact with the stratosphere. Air with elevated O_3 and a relatively negligible stratospheric component (less than 20%) is similar in composition to air arriving from Australia at midtropospheric levels. *Dibb et al.* [this issue] estimate that a significant fraction of biomass burning plumes were 5–14 days removed from the combustion source, a time range which allows polluted air parcels from Australia as well as South America and Africa to reach the South Pacific.

The distribution of the nine air mass types geographically and vertically was explained in part by the general meteorology of the study region. Low-O_3 air occurred predominantly in regions of convergence and deep convection, being distributed from the boundary layer where high water vapor and solar insolation promoted O_3 destruction. Low-O_3 air occupied ~30% of the troposphere between 10°N and 20°S latitude and longitudes west of 120°W, and 43% in the same latitude range east of 120 W. Enhanced O_3 layers resulting from biomass burning were observed on every flight over the South Pacific Ocean down to latitude 52°S. The prevailing westerly winds transported the majority of those layers into the midlatitude region with the highest levels of O_3 being greater than 100 ppbv. At midlatitudes, the biomass burning plumes with a relatively negligible stratospheric component occupied 28% of the troposphere in the western and central part of the study region, but even at low latitudes these plumes occupied 14–19% of the troposphere. Those biomass burning plumes having enhanced aerosol loading were restricted to altitudes below 9 km between latitudes 20°S and 40°S and longitudes west of 160°W, where they occupied ~12% of the troposphere in the altitude range 1–9 km. Enhanced O_3 layers with a stratospheric component occurred in or downwind of regions of subsidence, occupying >25% of the troposphere in the mid and high latitudes. In the eastern part of the study region, pollution from the Americas became important.

References

Anderson, B. E., et al., Aerosols from biomass burning over the tropical South Atlantic region: Distributions and impacts, *J. Geophys. Res.*, *101*, 24,117–24,137, 1996.

Blake, N. J., et al., Influence of southern hemispheric biomass burning on midtropospheric distributions of nonmethane hydrocarbons and selected halocarbons over the remote South Pacific, *J. Geophys. Res.*, this issue.

Board, A. S., H. E. Fuelberg, G. L. Gregory, B. G. Heikes, M. G. Schultz, D. R. Blake, J. E. Dibb, S.T. Sandholm, and R.W. Talbot, Chemical characteristics of air from differing source regions during PEM-Tropics A, *J. Geophys. Res.*, this issue.

Browell, E. V., Remote sensing of tropospheric gases and aerosols with an airborne DIAL system, in *Optical Laser Remote Sensing*, edited by D. K. Killinger and A. Mooradian, pp. 138–147, Springer-Verlag, New York, 1983.

Browell, E. V., Differential absorption lidar sensing of ozone, *Proc. IEEE*, *77*, 419–432, 1989.

Browell, E. V., A. F. Carter, S. T. Shipley, R. J. Allen, C. F. Butler, M. N. Mayo, J. H. Siviter Jr., and W. M. Hall, NASA multipurpose airborne DIAL system and measurements of ozone and aerosol profiles, *Appl. Opt.*, *22*, 522–534, 1983.

Browell, E. V., S. Ismail, and S. T. Shipley, Ultraviolet DIAL measurement of O_3 profiles in regions of spatially inhomogeneous aerosols, *Appl. Opt.*, *24*, 2827–2836, 1985a.

Browell, E. V., S. T. Shipley, C. F. Butler, and S. Ismail, Airborne lidar measurements of aerosols, mixed layer heights, and ozone during the 1980 PEPE/NEROS summer field experiment, *NASA Ref. Publ.*, RP-1143, 1985b.

Browell, E. V., E. F. Danielsen, S. Ismail, G. L. Gregory, and S. M. Beck, Tropopause fold structure determined from airborne lidar and in situ measurements, *J. Geophys. Res.*, *92*, 2112–2120, 1987.

Browell, E. V., et al., Large-scale air mass characteristics observed over western Pacific during summertime, *J. Geophys. Res.*, *101*, 1691–1712, 1996a.

Browell, E. V., et al., Ozone and aerosol distributions and air mass characteristics over the South Atlantic basin during the burning season, *J. Geophys. Res.*, *101*, 24,043–24,068, 1996b.

Browell, E.V., S. Ismail, and W. B. Grant, Differential absorption lidar (DIAL) measurements from air and space, *Appl. Phys. B*, *67*, 399–410, 1998.

Cahoon, D. R., B. J. Stocks, J. S. Levine, W. R. Cofer, and K. P. O'Neill, Seasonal distribution of African savanna fires, *Nature*, *359*, 812–815, 1992.

Collis, R. T. H., and P. B. Russell, Lidar measurments of particles and gases by elastic backscattering and differential absorption, in *Laser Monitoring of the Atmosphere*, edited by E. D. Hinkley, pp. 71–151, Springer-Verlag, New York, 1976.

Dibb, J. E., R. W. Talbot, E. M. Scheuer, D. R. Blake, N. J. Blake, G. L. Gregory, G. W. Sachse, and D. C. Thornton, Aerosol chemical composition and distribution during the Pacific Exploratory Mission, Tropics, *J. Geophys. Res.*, *104*, 5785–5800, 1999.

Dibb, J. E., R. W. Talbot, L. D. Meeker, E. M. Scheuer, N. J. Blake, and D. R. Blake, Constraints on the age and dilution of PEM-Tropics biomass burning plumes from the natural radionuclide tracer ^{210}Pb, *J. Geophys. Res.*, this issue.

Fenn, M. A., E. V. Browell, and C. F. Butler, Airborne lidar measurements of ozone and aerosols during PEM-West A and PEM-West B, in *Advances in Atmospheric Remote Sensing With Lidar*, edited by A. Ansmann, R. Neuber, P. Rairoux, and U. Wandinger, pp. 355–358, Springer-Verlag, New York, 1997.

Francey, R. J., L. P. Steele, R.L. Langenfelds, and B. C. Pak, High precision long-term monitoring of radiatively active and related trace

gases at surface sites and from aircraft in the southern hemisphere atmosphere, 1994–95, *J. Atmos. Sci.*, *56*, 279–285, 1999.

Fuelberg, H. E., R. O. Loring Jr., M. V. Watson, M. C. Sinha, K. E. Pickering, A. M. Thompson, G. W. Sachse, D. R. Blake, and M. R. Schoeberl, TRACE A trajectory intercomparison, 2, Isentropic and kinematic methods, *J. Geophys. Res.*, *101*, 23,927–23,939, 1996.

Fuelberg, H. E., R. E. Newell, S. Longmore, Y. Zhu, D. J. Westberg, E. V. Browell, D. R. Blake, G. R. Gregory, and G. W. Sachse, A meteorological overview of the PEM-Tropics Period, *J. Geophys. Res.*, *104*, 5585–5622, 1999.

Godfrey, J. S., R. A. Houze Jr., R. H. Johnson, R. Lukas, J. -L. Redelsperger, A. Sumi, and R. Weller, Coupled Ocean-Atmosphere Response Experiment (COARE): An interim report, *J. Geophys. Res.*, *103*, 14,395–14,450, 1998.

Hoell, J. M., D. D. Davis, D. J. Jacob, M. O. Rodgers, R. E. Newell, H. E. Fuelberg, R. J. McNeal, J. L. Raper, and R. J. Bendura, The Pacific Exploratory Mission in the tropical Pacific: PEM-Tropics A, August–September 1996, *J. Geophys. Res.*, *104*, 5567–5584, 1999.

Junge, C. E., *Air Chemistry and Radioactivity*, pp. 232–235, Academic, San Diego, Calif., 1963.

Kent, G. S., C. R. Trepte, K. M. Skeens, and D. M. Winker, LITE and SAGE II measurements of aerosols in the southern hemisphere upper troposphere, *J. Geophys. Res.*, *103*, 19,111–19,127, 1998.

Komala, N., S. Saraspriya, K. Kita, and T. Ogawa, Tropospheric ozone behavior observed in Indonesia, *Atmos. Environ.*, *30*, 1851–1856, 1996.

Li, Y., R. Ménard, L. P. Riishøjgaard, S. E. Cohn, and R. B. Rood, A study on assimilating PV data, *Tellus, Ser. A*, *50*, 490–506, 1998.

Mauzerall, D. L., et al., Photochemistry in biomass burning plumes and implications for tropospheric ozone over the tropical South Atlantic, *J. Geophys. Res.*, *103*, 8401–8423, 1998.

Newell, R. E., E. V. Browell, D. D. Davis, and S. C. Liu, Western Pacific tropospheric ozone and PV: Implications for Asian pollution, *Geophys. Res. Lett.*, *24*, 2733–2736, 1997.

Olson, J., B. Baum, D. Cahoon, and J. Crawford, The frequency and distribution of forest, savanna, and crop fires over tropical regions during PEM-Tropics A, *J. Geophys. Res*, *104*, 5865–5876, 1999.

O'Sullivan, D. W., B. G. Heikes, M. Lee, W. Chang, G. L. Gregory, D. R. Blake, and G. W. Sachse, The distribution of hydrogen peroxide and methylhydroperoxide over the Pacific and South Atlantic Oceans, *J. Geophys. Res.*, *104*, 5635–5646, 1999.

Richter, D. A., E. V. Browell, C. F. Butler, and N. S. Higdon, Advanced airborne UV DIAL system for stratospheric and tropospheric ozone and aerosol measurements, in *Advances in Atmospheric Remote Sensing With Lidar*, edited by A. Ansmann, R. Neuber, P. Rairoux, and U. Wandinger, pp. 395–398, Springer-Verlag, New York, 1997.

Schultz, M. G., et al., On the origin of tropospheric ozone and NO_x over the tropical South Pacific, *J. Geophys. Res.*, *104*, 5829–5844, 1999.

Talbot, R. W., J. E. Dibb, E. M. Scheuer, D. R. Blake, N. J. Blake, G. L. Gregory, G. W. Sachse, J. D. Bradshaw, S. T. Sandholm, and H. B. Singh, Influence of biomass combustion emissions on the distribution of acidic trace gases over the southern Pacific basin during austral springtime, *J. Geophys. Res.*, *104*, 5623–5634, 1999.

Thompson, A. M., et al., Ozone observations and a model of marine boundary layer photochemistry during SAGA 3, *J. Geophys. Res.*, *98*, 16,955–16,968, 1993.

Thornton, D. C., A. R. Bandy, B. W. Blomquist, A. R. Driedger, and T. P. Wade, Sulfur dioxide distribution over the Pacific Ocean 1991–1996, *J. Geophys. Res.*, *104*, 5845–5854, 1999.

Vay, S. A., B. E. Anderson, T. J. Conway, G. W. Sachse, J. E. Collins Jr., D. R. Blake, and D. J. Westberg, Airborne observations of the tropospheric CO_2 distribution and its controlling factors over the South Pacific Basin, *J. Geophys. Res.*, *104*, 5663–5676, 1999.

B. E. Anderson, E. V. Browell, C. F. Butler, M. B. Clayton, M. A. Fenn, W. B. Grant, G. L. Gregory, S. A. Kooi, and G. W. Sachse, NASA Langley Research Center, Hampton, VA 23681 (b.e.anderson@larc.nasa.gov; e.v.browell@larc.nasa.gov; c.f.butler@larc.nasa.gov; m.b.clayton@larc.nasa.gov; m.a.fenn@larc.nasa.gov; w.b.grant@larc.nasa.gov; g.l.gregory@larc.nasa.gov; s.a.kooi@larc.nasa.gov; g.w.sachse@larc.nasa.gov.)

A. R. Bandy and D. C. Thorton, Drexell University, Philadelphia, PA 19104. (arb@ac1.chemistry.drexel.edu; dct@ac2.chemistry.drexel.edu.)

D. R. Blake, Department of Chemistry, University of California, Irvine, CA 92717. (dblake@orion.oac.uci.edu.)

J. D. Bradshaw and S. T. Sandholm, Georgia Institute of Technology, Atlanta, GA 30332. (ss27@prism.gatech.edu.)

J. E. Dibb and R. W. Talbot, Institute for the Study of Earth, Oceans, and Space, University of New Hampshire, Durham, NH 03824. (Jack.Dibb@grg.sr.unh.edu; rwt@christa.unh.edu.)

H. E. Fuelberg, Department of Meteorology, Florida State University, Tallahassee, FL 32306. (fuelberg@huey.met.fsu.edu.)

B. G. Heikes, Graduate School of Oceanography, University of Rhode Island, Narrangansett, RI 02882. (zagar@notos.gso.uri.edu.)

R. E. Newell and Y. Zhu, Department of Earth, Atmospheric and Planetary Sciences, Massachusetts Institute of Technology, Cambridge, MA 02139. (newell@newell1.mit.edu; zhu@newell1.mit,edu.)

H. B. Singh, NASA Ames Research Center, Moffett Field, CA 94035. (hsingh@mail.arc.nasa.gov.)